Struct Multidisc Optim (2012) 45:717–728
DOI 10.1007/s00158-011-0737-5

RESEARCH PAPER

Optimization of vibrating structures to reduce radiated noise

Arup Kumar Nandy · C. S. Jog

Received: 6 September 2011 / Accepted: 23 October 2011 / Published online: 19 November 2011

Abstract In this work, we propose an approach for reducing radiated noise from 'light' fluid-loaded structures, such as, for example, vibrating structures in air. In this approach, we optimize the structure so as to minimize the dynamic compliance (defined as the input power) of the structure. We show that minimizing the dynamic compliance results in substantial reductions in the radiated sound power from the structure. The main advantage of this approach is that the redesign to minimize the dynamic compliance moves the natural frequencies of the structure away from the driving frequency thereby reducing the vibration levels of the structure, which in turn results in a reduction in the radiated sound power as an *indirect* benefit. Thus, the need for an acoustic and the associated sensitivity analysis is completely bypassed (although, in this work, we do carry out an acoustic analysis to demonstrate the reduction in sound power levels), making the strategy efficient compared to existing strategies in the literature which try to minimize some measure of noise directly. We show the effectiveness of the proposed approach by means of several examples involving both topology and stiffener optimization, for vibrating beam, plate and shell-type structures.

Keywords Optimization · Dynamic compliance · Manufacturability

A. K. Nandy · C. S. Jog (✉)
Facility for Research in Technical Acoustics (FRITA),
Mechanical Engineering Department,
Indian Institute of Science,
Bangalore 560012, India
e-mail: jogc@mecheng.iisc.ernet.in

1 Introduction

Due to its practical importance, the problem of redesigning a structure so as to minimize radiated sound levels has received a lot of attention in recent times; see, e.g., the book by Koopman and Fahnline (1997) and the comprehensive review articles by Christensen et al. (1998) and Marburg (2002b, 2004). Again, due to their practical importance, a vast majority of applications, have focused on 'light' fluid loading, e.g., a structure vibrating in air. In this case, the structural-acoustic analysis problem can be treated as a 'one-way' coupled one, i.e., the effects of the fluid loading are ignored while carrying out the structural analysis, and the obtained structural surface velocities are used as boundary conditions in the acoustic analysis. We shall focus on this case throughout this work. Indeed, this 'one-way' coupling is exploited in the proposed strategy in this work.

Lamancusa (1993) discusses several choices of design variables and objective functions that have been used, and concludes that the choice of acoustic power as an objective function produces the most consistently improved designs; examples of works where sound power is optimized are Belegundu et al. (1994), Koopman and Fahnline (1997), Constans et al. (1998), Milsted et al. (1993) and Du and Olhoff (2007). In the works of Koopman and Fahnline (1997) and Du and Olhoff (2007), general (i.e., valid for arbitrary structures) expressions for the sensitivities of the sound power with respect to design variables are derived, and subsequently used in the optimization strategy. However, such a sensitivity analysis and the associated optimization procedure is not only extremely cumbersome, but, is computationally intensive as well since both a structural and acoustic analysis has to be conducted at each iteration step (Milsted et al. 1993; Du and Olhoff 2007). Hence, Constans et al. (1998) and Milsted et al. (1993) use

non-gradient based approaches. However, such non-gradient approaches are also computationally intensive due to the large number of function evaluations that are required in such strategies.

Besides sound power, other objective functions and choices of design variables have also been used. For example, in the work of Marburg (2002a), the sound pressure level is optimized by directly manipulating the geometry of the shell finite element mesh, while in the works of Duhring et al. (2008) and Du and Olhoff (2010) the sound pressure level for interior and exterior problems, respectively, is optimized by using topology optimization (Eschenauer and Olhoff 2001; Bendsoe and Sigmund 2003). Note, however, that using an acoustic objective function different than sound power still necessitates a structural and acoustic analysis, and, thus, does not reduce the computational complexity of the optimization process.

Jog (2002a) proposed a method of reducing the vibrations of a structure by minimizing the dynamic compliance, which is defined as the average input power over a cycle. Such a minimization moves the natural frequencies of the structure away from the driving frequencies resulting in a reduction in the vibration levels, and hence, *indirectly*, to a reduction in the radiated sound power. Thus, as we show in this work, significant reductions in radiated sound power for 'light' fluid-loaded structures can be obtained simply by minimizing the dynamic compliance, thereby circumventing the need to conduct an acoustic analysis.[1] The proposed method works since the vibration of the structure is assumed not to be affected by the 'light' fluid (as is routinely done), and, obviously, this approach should not be used in cases where the fluid influences the vibration of the structure necessitating a fully coupled analysis. Nevertheless, since a vast majority of applications involve vibrations of structures in air, the proposed approach is likely to prove useful. Some preliminary results using this approach were presented by Jog (2002b, 2003) (where it was shown that minimizing the dynamic compliance also results in a reduction in the acoustic potential energy in interior acoustic problems). However, as Marburg (2002b) pointed out, this approach has not been tried for more complex structures. It is the goal of this work to show that this approach not only works for different types of plate- and shell-structures, but also that it works with different types of design variables such as 'density' type variables used in topology optimization, or more traditional ones such as the thickness of stiffeners. Although, obviously, topology optimization results in much larger sound power reductions, the latter type of design variables have also been used in this work since rib-stiffened shell structures may be easier to manufacture. Throughout this work, we consider only exterior acoustic problems, and both the structural and acoustic analysis are carried out using a finite element-based approach.

Similar to the comparison carried out by Jog (2002b), Du and Olhoff (2007) also compare the topologies obtained by minimizing the sound power directly, and by minimizing the dynamic compliance (although their definition of dynamic compliance is different than the one used by Jog 2002a). They found that for low frequencies the topologies are virtually indistinguishable, while for higher frequencies, the topologies are significantly different. However, even at the higher frequencies, they found (see their Table 1) that significant reductions in sound power levels (as compared to the starting-design sound power values) are obtained by merely minimizing the dynamic compliance, which provides further motivation for the approach followed in this work. Thus, even though direct sound power minimization may yield slightly better results, the indirect approach followed here may prove to be far more cost effective and simpler to use, since only a structural analysis is involved.

The outline of the remainder of this paper is as follows. In Section 2, we briefly discuss the acoustic analysis and optimization procedures that have been used. Sections 3 and 4 present the results using topology optimization and different kinds of stiffeners, respectively. Section 5 presents the conclusions.

2 Acoustic analysis and optimization formulations

2.1 Acoustic analysis

When the loading, and hence the pressure response is time harmonic, i.e., when

$$p = \tilde{p} e^{i\omega t}, \tag{1}$$

where ω is the angular frequency, the wave equation reduces to the Helmholtz equation,

$$\nabla^2 \tilde{p} + k^2 \tilde{p} = 0, \tag{2}$$

where $k = \omega/c$ is acoustic wave number, and c is acoustic wave speed. In an exterior radiation problem, the normal velocity v_n is specified over part of the boundary Γ_r, while over the part of the boundary Γ_∞ where the domain is truncated, appropriate absorbing conditions that approximate the Sommerfeld radiation condition are specified. On Γ_r, the boundary condition is given by

$$\nabla \tilde{p} \cdot \boldsymbol{n} = -\rho_f i\omega v_n, \tag{3}$$

where ρ_f denotes the density of the acoustic fluid.

[1] Although we do conduct an acoustic analysis in this work, it is carried out merely to demonstrate the significant reduction in sound power levels that result by using the proposed method.

We take Γ_∞ to be a sphere of radius R throughout this work, and use a spherical damper of the form (Bayliss and Turkel 1980)

$$\nabla \tilde{p} \cdot \boldsymbol{n} = -\frac{\tilde{p}}{R} - ik\tilde{p}. \tag{4}$$

The finite element formulation is obtained by discretizing the pressure field as

$$\tilde{p} = \boldsymbol{N}_p \hat{\boldsymbol{p}}, \tag{5}$$

$$\nabla \tilde{p} = \boldsymbol{B}_p \hat{\boldsymbol{p}}, \tag{6}$$

where $\boldsymbol{N}_p = [N_1\, N_2 \ldots]$ is the standard Lagrange shape function matrix, and

$$\boldsymbol{B}_p = \begin{bmatrix} \frac{\partial N_1}{\partial x} & \frac{\partial N_2}{\partial x} & \cdots \\ \frac{\partial N_1}{\partial y} & \frac{\partial N_2}{\partial y} & \cdots \\ \frac{\partial N_1}{\partial z} & \frac{\partial N_2}{\partial z} & \cdots \end{bmatrix}. \tag{7}$$

The conventional finite element matrix formulation is given by

$$\left[\boldsymbol{K}_p - \omega^2 \boldsymbol{M}_p + i\omega \boldsymbol{C}_p\right] \hat{\boldsymbol{p}} = \hat{\boldsymbol{f}}_p, \tag{8}$$

where, with R written as $|\boldsymbol{x}|$,

$$\boldsymbol{K}_p = \int_\Omega \boldsymbol{B}_p^T \boldsymbol{B}_p \,\mathrm{d}\Omega + \int_{\Gamma_\infty} \frac{1}{|\boldsymbol{x}|} \boldsymbol{N}_p^T \boldsymbol{N}_p \,\mathrm{d}\Gamma,$$

$$\boldsymbol{M}_p = \int_\Omega \frac{1}{c^2} \boldsymbol{N}_p^T \boldsymbol{N}_p \,\mathrm{d}\Omega,$$

$$\boldsymbol{C}_p = \int_{\Gamma_\infty} \frac{1}{c} \boldsymbol{N}_p^T \boldsymbol{N}_p \,\mathrm{d}\Gamma,$$

$$\hat{\boldsymbol{f}}_p = -\int_{\Gamma_r} \rho_f i\omega v_n \boldsymbol{N}_p^T \,\mathrm{d}\Gamma.$$

Since only outgoing waves are present in exterior acoustic problems, we can devise a more efficient finite element strategy by assuming the pressure to be of the form

$$\tilde{p} = \frac{1}{|\boldsymbol{x}|} G(\boldsymbol{x}) \mathrm{e}^{-ik|\boldsymbol{x}|} \tag{9}$$

where $|\boldsymbol{x}| = \sqrt{\boldsymbol{x} \cdot \boldsymbol{x}}$, and $G(\boldsymbol{x})$ is an unknown function which is to be determined by an approximation strategy such as the finite element method. Note that the above form provides a bias towards outgoing waves, and also satisfies the spherical damping condition given by (4). Since the oscillatory part is separated out, the resulting finite element formulation has to capture a relatively gently varying function, and, thus, a much coarser mesh can be used.

Substituting (9) in (2) and using (4), the governing differential equation and boundary condition for $G(\boldsymbol{x})$, and subsequently the finite element formulation, can be derived. Discretizing $G(\boldsymbol{x})$ as

$$G = \boldsymbol{N}_p \hat{\boldsymbol{g}}, \tag{10}$$

$$\nabla G = \boldsymbol{B}_p \hat{\boldsymbol{g}}, \tag{11}$$

with $\boldsymbol{B}_p$ given by (7), we obtain the finite element equations as

$$\left[\boldsymbol{K}_g + i\omega \boldsymbol{C}_g\right] \hat{\boldsymbol{g}} = \hat{\boldsymbol{f}}_g, \tag{12}$$

where

$$\boldsymbol{K}_g = \int_\Omega \left[\boldsymbol{B}_p^T \boldsymbol{B}_p + \frac{2}{|\boldsymbol{x}|^2} \boldsymbol{N}_p^T \boldsymbol{x}^T \boldsymbol{B}_p\right] \mathrm{d}\Omega - \int_{\Gamma_r} \frac{\boldsymbol{x} \cdot \boldsymbol{n}}{|\boldsymbol{x}|^2} \boldsymbol{N}_p^T \boldsymbol{N}_p \,\mathrm{d}\Gamma,$$

$$\boldsymbol{C}_g = \int_\Omega \frac{2}{c\,|\boldsymbol{x}|} \boldsymbol{N}_p^T \boldsymbol{x}^T \boldsymbol{B}_p \,\mathrm{d}\Omega - \int_{\Gamma_r} \frac{\boldsymbol{x} \cdot \boldsymbol{n}}{c\,|\boldsymbol{x}|} \boldsymbol{N}_p^T \boldsymbol{N}_p \,\mathrm{d}\Gamma,$$

$$\hat{\boldsymbol{f}}_g = -\int_{\Gamma_r} \rho_f i\omega v_n\, |\boldsymbol{x}|\, \mathrm{e}^{ik|\boldsymbol{x}|} \boldsymbol{N}_p^T \,\mathrm{d}\Gamma.$$

Note that there is no boundary term over the boundary Γ_∞. If the origin is not part of the acoustic domain, then the above elements can be used directly in the vicinity of the radiator, while if the origin is part of the acoustic domain, then we use conventional elements in the vicinity of the origin, and the proposed elements beyond that.

2.2 Objective function–dynamic compliance

The finite element structural equations under harmonic loading $\boldsymbol{f}_0 \cos \hat{\omega} t$ can be written as

$$\left[\boldsymbol{K} - \hat{\omega}^2 \boldsymbol{M} + i\hat{\omega} \boldsymbol{C}\right] (\boldsymbol{x}_r + i\boldsymbol{x}_s) = \boldsymbol{f}_0,$$

where $\boldsymbol{K}$, $\boldsymbol{M}$ and $\boldsymbol{C}$ are the stiffness, mass and damping matrices, respectively. The displacement $\boldsymbol{u}$ is given by the real part of $(\boldsymbol{x}_r + i\boldsymbol{x}_s)e^{i\hat{\omega}t}$, and the velocity $\boldsymbol{v}$ is given by $\dot{\boldsymbol{u}}$. The dynamic compliance, defined as the average input power over a cycle, is given by Jog (2002a)

$$\begin{aligned} J_d &= -\frac{\hat{\omega}}{2\pi} \left[\int_0^{2\pi/\hat{\omega}} (\boldsymbol{f}_0 \cos \hat{\omega} t) \cdot \boldsymbol{v}\, dt\right] \\ &= -\frac{\hat{\omega}}{2} \boldsymbol{f}_0 \cdot \boldsymbol{x}_s \\ &= \frac{1}{2} \boldsymbol{x}_s \cdot \bar{\boldsymbol{K}} \boldsymbol{x}_s \\ &= -\Pi(\boldsymbol{x}_s), \end{aligned}$$

where

$$\bar{\boldsymbol{K}} = \left(\boldsymbol{K} - \hat{\omega}^2 \boldsymbol{M}\right) \boldsymbol{C}^{-1} \left(\boldsymbol{K} - \hat{\omega}^2 \boldsymbol{M}\right) + \hat{\omega}^2 \boldsymbol{C},$$

and the functional Π is given by

$$\Pi(\boldsymbol{y}) = \frac{1}{2} \boldsymbol{y} \cdot \bar{\boldsymbol{K}} \boldsymbol{y} + \hat{\omega} \boldsymbol{y} \cdot \boldsymbol{f}_0.$$

The optimization problem can be written as:

Find the vector of optimum design variables $\boldsymbol{\rho}^*$, and the vector of associated displacement-type variables $\boldsymbol{x}_s$, that solves

$$\max_{\boldsymbol{\rho}} \min_{\boldsymbol{y}} \Pi(\boldsymbol{\rho}, \boldsymbol{y}),$$

subject to the volume constraint

$$V = \sum_{i=1}^{N} \left(\frac{\rho_i}{\rho_s}\right) V_i \leq \bar{V}, \tag{13}$$

where N is the number of elements, ρ_i, $0 < \rho_i \leq 1$, is the density of the ith element, ρ_s is the value of the design variables in the starting design; we use a value of ρ_s which is equal to the volume fraction. V_i is the element volume in the starting design, and $\bar{V}$ is the specified volume. When stiffeners are being used, ρ_i can be interpreted as a measure of the thickness of the stiffeners, i.e.,

$$\frac{\text{Thickness}}{\text{Starting Thickness}} = \frac{\rho_i}{\rho_s}. \tag{14}$$

With this interpretation, we multiply the Young modulus in the stiffness matrix by $(\rho_i/\rho_s)^3$, and the density in the mass matrix by ρ_i/ρ_s.

The inner subproblem in the above optimization problem solves the problem of finding the displacement-type variables $\boldsymbol{x}_s$, for a given set of design variables, $\boldsymbol{\rho}$, while the outer subproblem solves the problem of minimizing the power input. The sensitivity of the objective function with respect to the design variables is given by

$$\frac{d\Pi}{d\rho_i} = \frac{\hat{\omega}^2}{2} \left[\boldsymbol{x}_s \cdot \frac{\partial \boldsymbol{C}}{\partial \rho_i} \boldsymbol{x}_s - \boldsymbol{x}_r \cdot \frac{\partial \boldsymbol{C}}{\partial \rho_i} \boldsymbol{x}_r \right] - \hat{\omega} \boldsymbol{x}_r \cdot \left(\frac{\partial \boldsymbol{K}}{\partial \rho_i} - \hat{\omega}^2 \frac{\partial \boldsymbol{M}}{\partial \rho_i} \right) \boldsymbol{x}_s. \tag{15}$$

Note that once the finite element analysis has been conducted, the sensitivity computation is quite trivial due to the explicit expression given above.

Since we consider only one constraint in this work, we use the optimality criteria method. The design variables are updated using the following modified optimality criterion method (Ma et al. 1995):

$$(\rho_i)^{\text{new}} = (\rho_i)^{\text{old}} \left[\frac{\rho_s \frac{d\pi}{d\rho_i} + \mu v_i}{(\Lambda + \mu) v_i} \right]^{\eta}, \quad i = 1 \text{ to N}. \tag{16}$$

The Lagrange multiplier Λ associated with the volume constraint is initially chosen arbitrarily. The parameter μ which ensures that the numerator is positive is found using

$$\mu = \begin{cases} 0 & \text{if all } \frac{d\pi}{d\rho_i} \geq 0, \\ -\min \left(\frac{d\Pi}{d\rho_i} \right) \frac{\rho_s}{v_i} & \text{for } \frac{d\pi}{d\rho_i} \leq 0. \end{cases} \tag{17}$$

The parameter η, which lies between 0 and 1, controls the rate of convergence–a value of 0.5 is used in this work. If the update process leads to density values greater than 1 or less than a minimum specified value (we have used a value of 0.01), then it is assigned a value of 1 or 0.01. Using the updated values of the design variables, V is calculated using (13). The Lagrange multiplier Λ is modified using a bisection method until the updated design satisfies the volume constraint given by (13) within a specified tolerance. We compare these updated density variables with the ones from the previous optimization cycle, and if the maximum difference is less than a specified tolerance, the process is considered to have converged, while otherwise, the next analysis and optimization update is carried out. In some cases, the μ value found using (17) leads to a very low value of Λ. In such a case, the value of μ is increased gradually (say, by a factor of 1.5) until a reasonable value of Λ results.

3 Topology optimization

Because of the ease of meshing with tetrahedral elements, both the structural and acoustic domains are meshed using 10 node tetrahedral elements. We use the Rayleigh (or proportional) damping model whereby

$$\boldsymbol{C} = \alpha \boldsymbol{M} + \beta \boldsymbol{K}.$$

The constants α and β are given by

$$\alpha = \frac{2\omega_1 \omega_2 (\xi_1 \omega_2 - \xi_2 \omega_1)}{\omega_2^2 - \omega_1^2},$$

$$\beta = \frac{2 (\xi_2 \omega_2 - \xi_1 \omega_1)}{\omega_2^2 - \omega_1^2},$$

where ξ_1 and ξ_2 are modal damping parameters corresponding to two distinct modes with natural frequencies ω_1 and ω_2. ω_1 is usually chosen to be the lowest natural frequency,

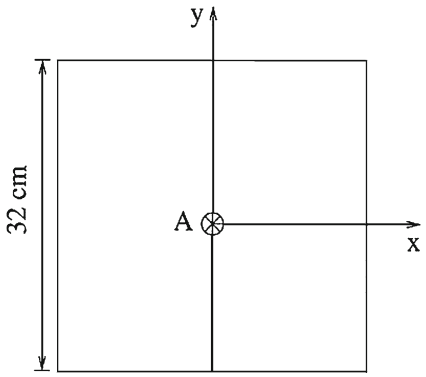

Fig. 1 Geometry and loading for the plate topology optimization problem

and ω_2 is chosen to be the smallest natural frequency greater than the highest loading frequency. Throughout the optimization procedure, the damping parameters ξ_1 and ξ_2 are assumed to be constant.

Since degenerate structures can result with topology optimization (e.g., see the optimal topology shown in Fig. 2 in Jog (2002a) in the case when the driving frequency is higher than the first natural frequency), we optimize the topology in a layer over a solid base plate or shell (alternatively, one could choose a high value of $\rho_{\min}$). The thickness and material properties of this layer are assumed to be the same as that of the base structure.

3.1 Topology optimization of a square plate

The geometry and loading for the square plate are shown in Fig. 1. The thickness of the base plate and top layer is 1 cm each. The Young modulus, Poisson ratio and density are $E = 210$ GPa, $\nu = 0.25$, and $\rho = 7800$ kg/m^3. The loading at the center of the plate structure (point A) is $80 \cos \hat{\omega} t$ N. All the four boundaries are simply supported. The specified volume fraction is 40%. The optimal topology

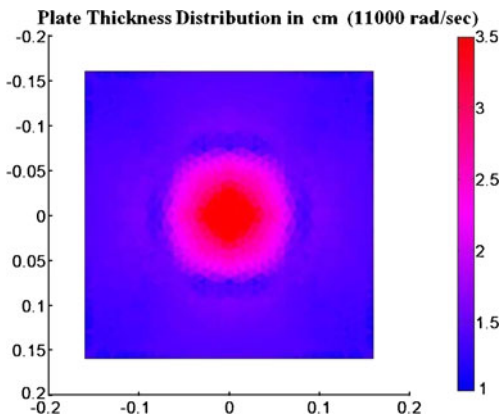

Fig. 2 Optimal topology for plate structure

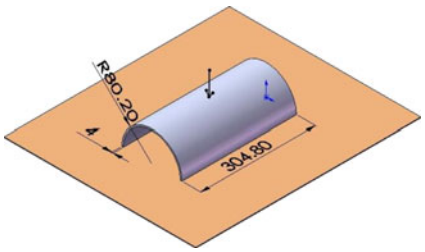

Fig. 3 Geometry and loading for shell topology optimization problem

is shown in Fig. 2. The input power reduces from 1.013 mW to 0.379 mW, while the acoustic sound power reduces from 17.28 μW to 5.388 μW.

3.2 Topology optimization of a shell structure

The geometry and loading are as shown in Fig. 3. The inner radius and thickness of the shell structure are 76.2 mm and 2 mm, respectively. The thickness of the base shell and top layer is 2 mm each. The material properties are $E = 71.1$ GPa, $\nu = 0.31$, and $\rho = 2790$ kg/m^3. The loading at the center of the shell structure is $0.8 \cos \hat{\omega} t$ N. The specified volume fraction is 40%. The two faces which are in contact with the base are assumed to be clamped. The optimal topology is shown in Fig. 4. The input power reduces from 0.229 μW to 0.091 μW, while the acoustic sound power reduces from 0.727×10^{-4} μW to 0.2392×10^{-4} μW.

Since optimal topologies, such as the ones shown in Figs. 2 and 4, may be difficult to manufacture, we now consider the optimization of stiffeners (or liners) that are attached to a base structure that is kept unchanged. The thickness of the stiffeners, which, due to manufacturability considerations is assumed to be constant over a given stiffener, is taken to be the design variable.

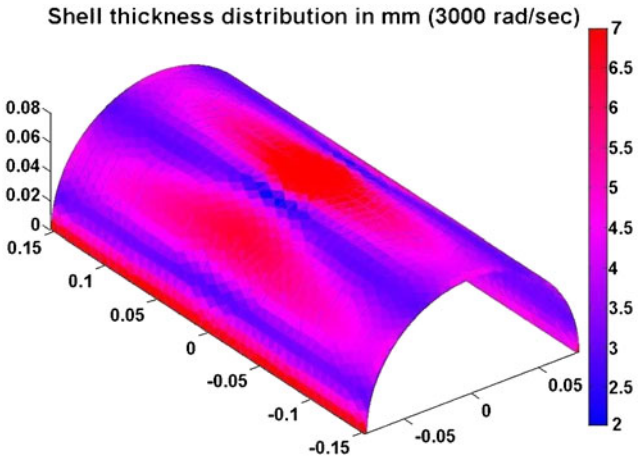

Fig. 4 Optimal topology of shell structure

4 Optimization with thickness of stiffeners as design variables

Since the thickness of a given stiffener is assumed to be constant, the number of design variables is equal to the number of stiffeners. In order to meet this constraint of constant thickness for a given stiffener, 'linking' of the design variables associated with each stiffener is carried out, i.e., the sensitivity with respect to the thickness for a stiffener is equal to the sum of the sensitivities with respect to the thickness for each finite element in the stiffener.

With the aforementioned formulation, each ρ_i can have any value between 0.01 and 1. However, since stiffeners are typically manufactured with standard thicknesses, each ρ_i value is rounded off to the nearest value in the set (0, 0.2, 0.4, 0.6, 0.8, 1) (we have verified that this rounding procedure results in very small changes in the input and acoustic powers as compared to the continuous case). The corresponding thickness is obtained using (14). This discrete model is then meshed, and a structural-acoustic analysis is conducted to verify that the acoustic power has reduced.

4.1 Cantilever beam problem

The dimension and boundary conditions are as shown in Fig. 5. The material properties are $E = 2.1 \times 10^{11}$ N/m^2, $\nu = 0.25$ and $\rho = 7800$ kg/m^3. The loading at the free edge is $1.5 \cos \omega t$ N/cm. The thickness of the base structure is 1 mm.

Stiffeners can be arranged either along the transverse or longitudinal directions. In order to allow a comparison of results, the dimension and number of liners have been chosen in such a way that the total volume (i.e.,volume of the base beam + volume of liners) is the same in both the transverse and longitudinal cases (see Figs. 6a and b). In the transverse case, the first liner is placed at a distance 0.004 m from the fixed end, and the inter-liner spacing is also the same. Each liner has a dimension (width × length × thickness) of 0.012 m × 0.006 m × 0.001 m. Thus, there are a total of 10 liners.

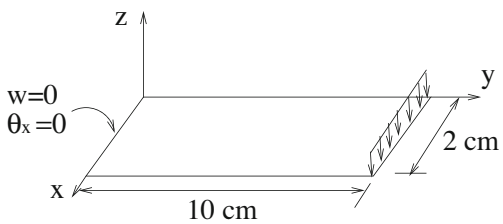

Fig. 5 Cantilever beam problem geometry

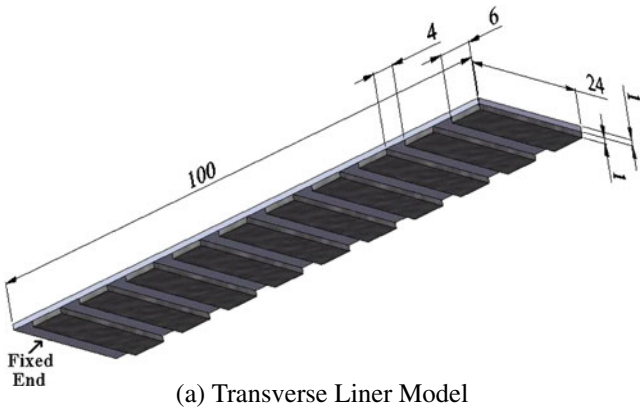

(a) Transverse Liner Model

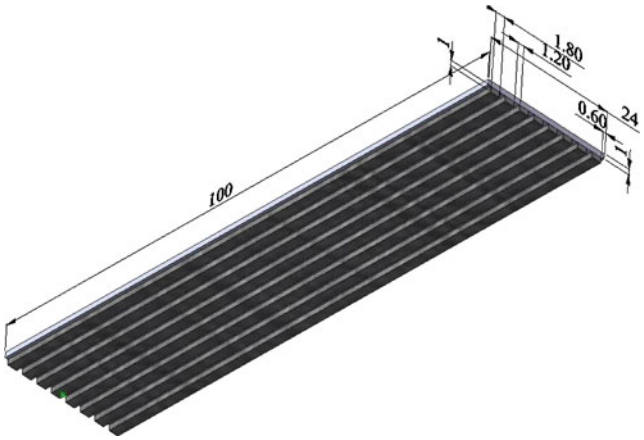

(b) Longitudinal Stiffener Model

Fig. 6 Stiffener arrangements in the starting designs of the beam (dimensions are in mm)

In the longitudinal case, the stiffeners are also assumed to be fixed into the wall. The first stiffener is at a distance of 0.0006 m from the symmetry plane. Each stiffener has a dimension of 0.0018 m × 0.1 m × 0.001 m. In this way 4 stiffeners can be placed with an inter-liner spacing of 0.0012 m. The first three natural frequencies of the starting transverse-stiffener model are 561, 3518 and 9871 rad/s, while those for the starting longitudinal-stiffener model are 1033, 6461 and 18055 rad/s. The two loading frequencies under which we carry out the optimization are 500 and 5000 rad/s. Note that the first driving frequency is less, while the second one is greater, than the first natural frequency of both the starting designs.

Table 1 shows the input and acoustic powers of the starting and optimal designs for both geometries and for both loading frequencies.

The results can be summarized as follows:

1. $\hat{\omega} = 500$ rad/s: With the use of transverse stiffeners, there is only a 10.26% reduction in input power, and the optimized design is almost the same as the starting design. However, with the use of longitudinal stiffeners,

Table 1 Comparison of input and acoustic sound powers for different beam-stiffener models

Loading frequency (rad/s)	Base beam Power (mW)	Transverse liners Starting power (mW)	Transverse liners Optimized power (mW)	Longitudinal stiffeners Starting power (mW)	Longitudinal stiffeners Optimized power (mW)
Input power					
500	3193.7	565.02	507.5	6.724	0.555
5000	8.584	5.527	1.373	11.229	2.226
Acoustic sound power					
500	7.426	0.7726	0.6976	4.975×10^{-3}	0.3085×10^{-3}
5000	0.0404	0.0166	0.0037	0.1685	0.0861

there is a reduction of 92% in the input power. As seen in Fig. 7, only two out of eight starting stiffeners, having thickness four times of the starting thickness, remain.

2. $\hat{\omega} = 5000$ rad/s: With the use of transverse stiffeners, there is a 75.16% reduction in input power and 77.71% reduction in sound power. The optimal design is shown in Fig. 8. With the use of longitudinal stiffeners, although there is an input-power reduction of 80.1% with respect to the stiffened starting design, there is an *increase* in input power with respect to the base design (see Table 1), thus, showing that longitudinal stiffeners are inappropriate for this frequency.

Thus, the optimization strategy shows that longitudinal stiffeners are appropriate for the case $\hat{\omega} = 500$ rad/s, while transverse stiffeners are appropriate for the case $\hat{\omega} = 5000$ rad/s. Table 2 shows that the natural frequencies of the starting design are pushed apart from the driving frequency as a result of the optimization, thus, reducing the dynamic

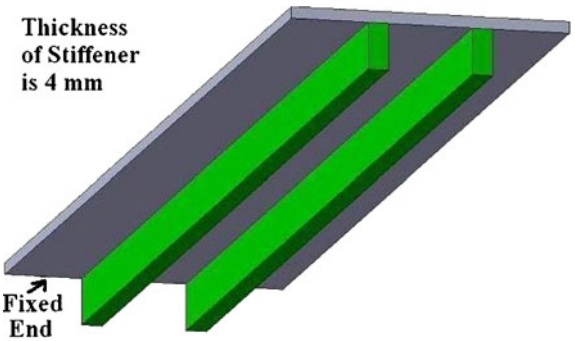

(a) Optimal design

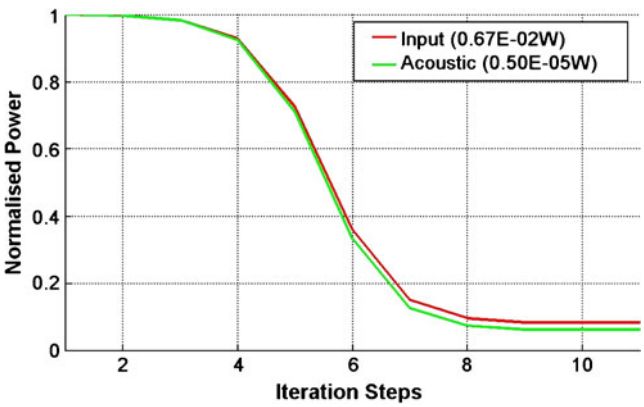

(b) Optimization of power

Fig. 7 Optimal longitudinal-stiffener design and associated power graph at driving frequency 500 rad/s; in this and subsequent figures, the power values are normalized against their starting values shown in parenthesis

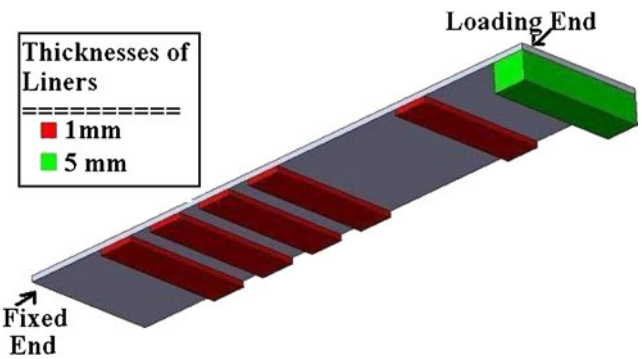

(a) Optimal design

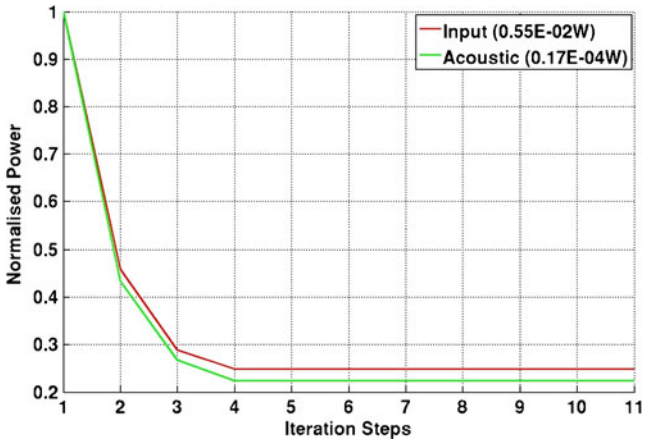

(b) Optimization of power

Fig. 8 Optimal transverse-stiffener design and associated power graph at driving frequency 5000 rad/s

Table 2 Effect of optimization on natural frequencies for different beam-stiffener models

Design	Natural frequencies (rad/s)		
	1st	2nd	3rd
	Base beam		
	534.8	3362.0	9514.0
	Transverse model		
Starting	561	3518	9871
Optimized (500)	564	3523	9871
Optimized (5000)	415	2719	8449
	Longitudinal model		
Starting	1033	6461	18055
Optimized (500)	1877	11497	31014
Optimized (5000)	1815	10987	28947

compliance, and, indirectly, the radiated sound power. As already noted, transverse stiffeners are ineffective for the case $\hat{\omega} = 500$ rad/s, and this is also seen from Table 2 where the natural frequencies move away from the driving frequency by a small amount.

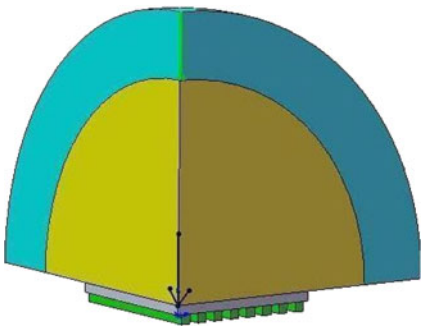

(a) Plate with stiffeners and the associated acoustic domain

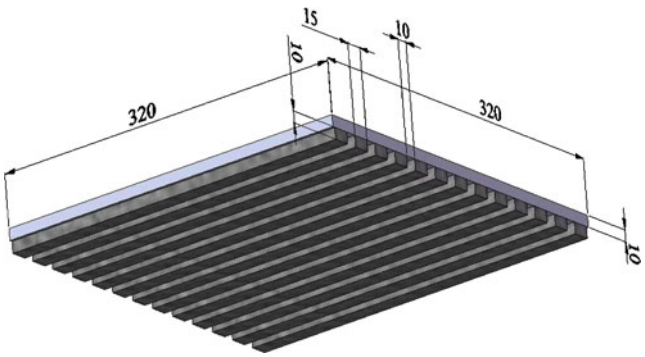

(b) Details of the stiffener arrangement (dimensions are in mm)

Fig. 9 The acoustic domain and stiffener arrangement for the plate problem

Table 3 Comparison of input and acoustic powers for different loading frequencies

Loading frequency (rad/s)	Starting design	Optimized design
Input power (mW)		
2000	2.42	0.832
11000	7.38	4.68
Acoustic sound power (mW)		
2000	0.0304	0.0077
11000	0.1146	0.089

4.2 Plate problem

The problem considered in Section 3 (see Fig. 1) is again considered here, but now with the use of stiffeners as design variables instead of topology optimization. Only one-fourth of the domain is modeled due to symmetry considerations. For conducting the acoustic analysis, inner and outer spherical acoustic domains, having radii 0.3 and 0.5 m respectively, are modelled over the plate top surface as shown in Fig. 9a. Conventional and the 'biased' finite elements

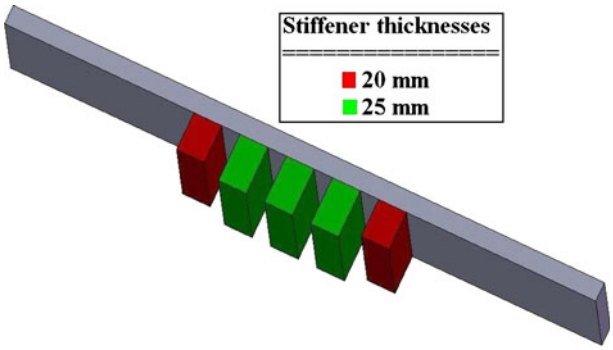

(a) Optimal design

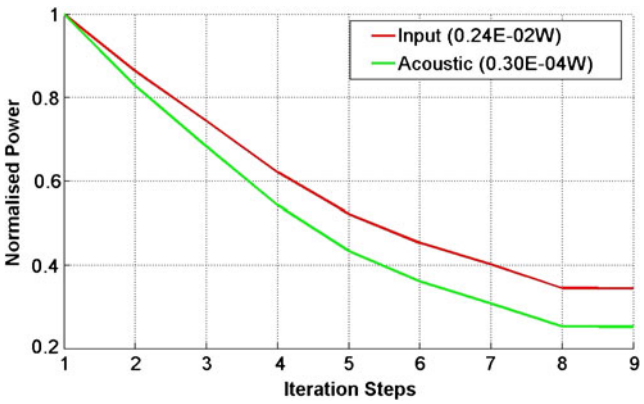

(b) Optimization of power

Fig. 10 Optimal design of stiffened plate and associated power graph at driving frequency 2000 rad/s

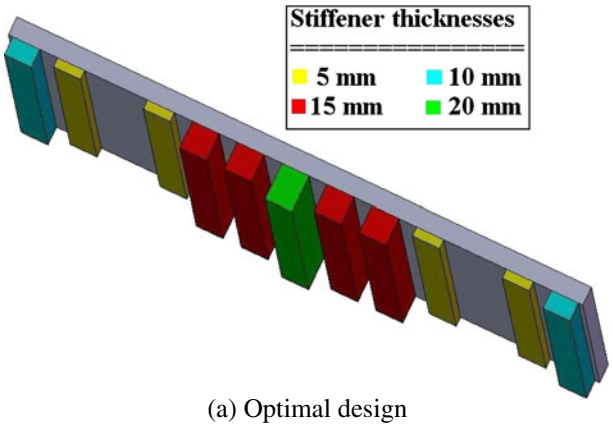

(a) Optimal design

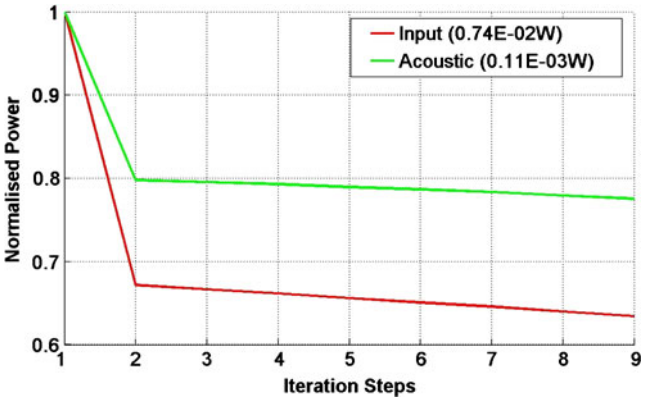

(b) Optimization of power

Fig. 11 Optimal design of stiffened plate and associated power graph at driving frequency 11000 rad/s

described in Section 2.1 are used in the inner and outer domains, respectively.

The stiffeners shown in Fig. 9b have a cross-section (thickness × width) of 1 × 1.5cm. The spacing between them is 1 cm, and a total of 13 stiffeners are used for the entire plate. The first three natural frequencies of the starting design shown in Fig. 9b are 3948, 14196 and 24913 rad/s. The two different loading frequencies considered are 2000 and 11000 rad/s. The volume fraction for both loading frequencies is taken to be 40%.

Table 3 presents the results for the input and acoustic powers for the starting and optimized designs for both loading frequencies. The optimal designs and associated power graphs for the two frequencies are shown in Figs. 10 and 11. In both cases, the central stiffener in the optimal design has the maximum thickness.

Table 4 presents the effect of optimization on the natural frequencies. In both cases, the natural frequencies in the neighborhood of the driving frequency are moved away from the driving frequency, once again showing that the dynamic compliance is an effective measure for reducing vibrations.

Table 4 Effect of optimization on the natural frequencies for the plate-stiffener problem

Design	Natural frequencies (rad/s)		
	1st	2nd	3rd
Starting	3948	14196	24913
Optimized (2000)	4615	10468	10481
Optimized (11000)	4264	10481	10542

4.3 Shell problem

The shell problem described in Section 3 (see Fig. 3) is revisited here in the context of stiffener optimization. As in the beam example, we consider transverse and longitudinal stiffeners (see Fig. 12). Once again, in order to facilitate a comparison of results, the number of stiffeners and their dimensions in the two cases are chosen such that the total volume of the base shell and stiffeners is the same. The radii

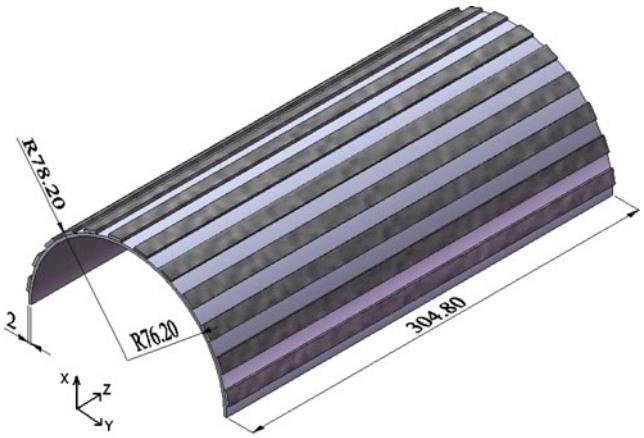

(a) Longitudinal-stiffener model

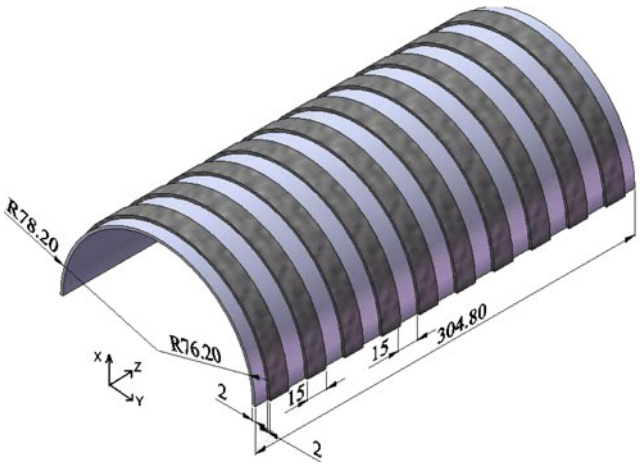

(b) Transverse-stiffener model

Fig. 12 Starting design for the shell-stiffener optimization problem (dimensions shown are in mm)

Table 5 Comparison of input and acoustic powers for different shell stiffener models

Loading frequency (rad/s)	Base shell Power (μW)	Transverse stiffeners Starting power (μW)	Transverse stiffeners Optimized power (μW)	Longitudinal stiffeners Starting power (μW)	Longitudinal stiffeners Optimized power (μW)
Input power					
3000	8.475	0.942	0.412	6.08	5.97
9000	25.561	2362.5	2249.4	15.774	9.408
Acoustic sound power					
3000	10.31×10^{-3}	0.369×10^{-3}	0.125×10^{-3}	6.1×10^{-3}	6×10^{-3}
9000	1.448	218.87	208.45	0.783	0.556

of the inner and outer acoustic domains are chosen as 0.2 m and 0.4 m, respectively. Due to symmetry, only one fourth of the domain is modeled and meshed.

In the quarter domain, the dimensions of each longitudinal stiffener along the r-θ-z directions are 0.002, 0.01 and 0.1524 m. The first stiffener is placed at a distance 0.005 m (along the arc) from the $y = 0$ symmetry plane. Six stiffeners placed 0.01 m apart (see Fig. 12a) are used. For the (quarter) transverse model, the dimensions along the r-θ-z directions are 0.002, 0.1228 and 0.015 m. The first stiffener is placed at a distance 0.0075 m from the z-symmetry plane (along the length of shell), and a total of five stiffeners are used with an inter-stiffener spacing of 0.015 m (see Fig. 12b).

The first three natural frequencies for the starting transverse-stiffener model are 8874, 15962 and 24870 rad/s, while those for the starting longitudinal-stiffener model are 5059, 14138 and 14487 rad/s. The two loading frequencies considered are 3000 and 9000 rad/s. Table 5 presents a comparison of the input and acoustic sound powers for the two

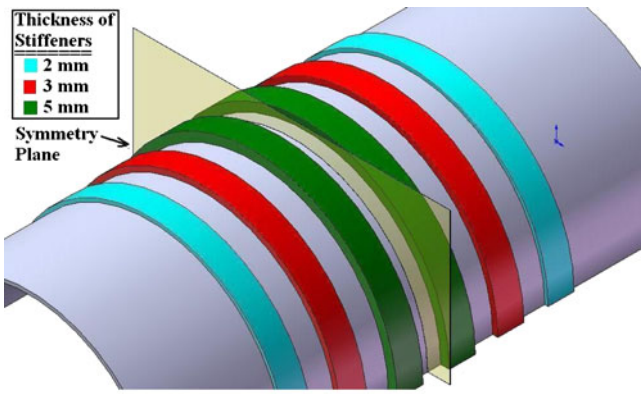

(a) Optimal design

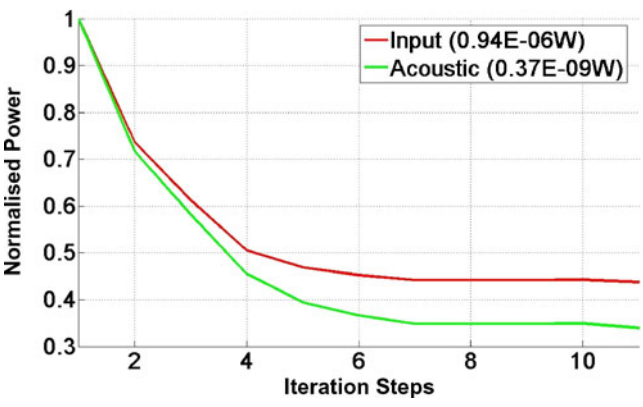

(b) Optimization of power

Fig. 13 Optimized shell design with transverse stiffeners for driving frequency 3000 rad/s

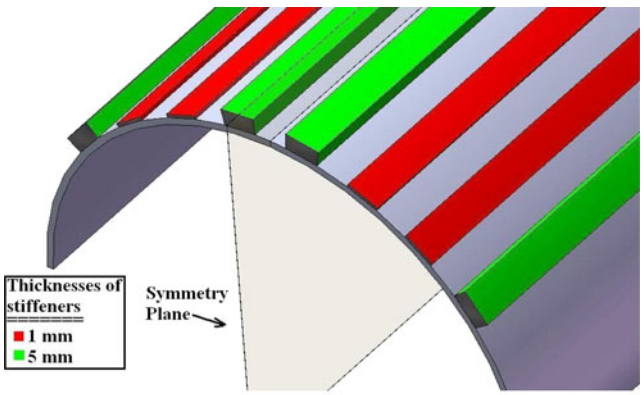

(a) Optimal design

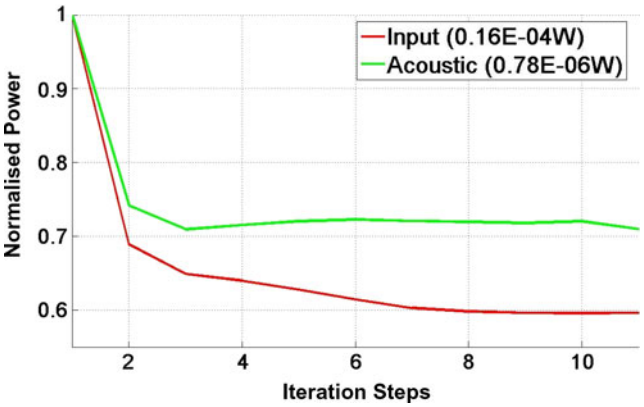

(b) Optimization of power

Fig. 14 Optimized shell design with longitudinal stiffeners for driving frequency 9000 rad/s

Table 6 Effect of optimization on natural frequencies for the transverse and longitudinal-stiffener models

Design	Natural frequencies (rad/s)		
	1st	2nd	3rd
	Base shell		
	5145	13529	14942
	Transverse model		
Starting	8874	15962	24870
Optimized (3000)	9510	15115	19482
Optimized (9000)	8868	15959	24856
	Longitudinal model		
Starting	5059	14138	14487
Optimized (3000)	5088	14007	14455
Optimized (9000)	4374	14030	15854

models with those of the base shell and the starting design. In contrast to the conclusions for the beam example, we find in this case that the transverse stiffeners are more effective than longitudinal ones for the lower frequency, and vice-versa for the higher frequency. In fact, for the case $\hat{\omega} = 9000$ rad/s, addition of transverse stiffeners worsens the performance relative to the base shell by a factor of about 100! Thus, the intuitive idea that 'addition of stiffeners reduces vibration levels' can be dramatically wrong (depending on the driving frequency for a given structure), and shows the importance of using the dynamic compliance for measuring vibration levels of the structure. The optimal designs using transverse and longitudinal stiffeners for the lower and higher driving frequencies, respectively, are shown in Fig. 13 and 14. As can be seen from the associated power graphs, they result in very significant reductions in both the input and sound powers.

Table 6 shows the very significant shifting of the natural frequencies away from the driving frequency with the use of transverse stiffeners when $\hat{\omega} = 3000$ rad/s, and longitudinal ones when $\hat{\omega} = 9000$ rad/s.

5 Conclusions

We now summarize the findings of this work.

1. In the case of light-fluid loaded structures, such as structures vibrating in air, we have shown in the case of beam, plate and shell structures, that significant reductions in sound-power levels can result as an *indirect* benefit of minimizing the dynamic compliance of the structure, due to the fact that this process of optimization moves the natural frequencies of the structure in the vicinity of the driving frequency away from the driving frequency. Since only a structural analysis needs to be conducted, and since analytical sensitivities are used, the whole procedure is extremely efficient, and bypasses the need for an acoustic, and the associated (and quite complicated) sensitivity analysis that is required in minimizing acoustic performance measures (such as sound pressure levels or acoustic power) directly.
2. Although it is well known that topology optimization can result in significant reductions in a performance functional, we have shown in this work that using alternative design variables such as stiffeners can also lead to significant reductions in the dynamic compliance. This is important from the viewpoint of manufacturability.
3. For a particular driving frequency, merely adding stiffeners may worsen the situation relative to the base structure, resulting in significantly increased vibration levels. Thus, a systematic approach such as the one outlined in this work needs to be used, not only for finding the optimal dimensions of the stiffeners, but also their optimal placement.

References

Bayliss A, Turkel E (1980) Radiation boundary conditions for wave-like equations. Commun Pure Appl Math XXXIII:707–725

Belegundu AD, Salagame RR, Koopmann GH (1994) A general optimization strategy for sound power minimization. Struct Optim 8:113–119

Bendsoe MP, Sigmund O (2003) Topology optimization: theory, methods and applications. Springer, Berlin

Christensen ST, Sorokin SV, Olhoff N (1998) On analysis and optimization in structural acoustics—part I: problem formulation and solution techniques. Struct Optim 16:83–95

Constans EW, Belegundu AD, Koopman GH (1998) Design approach for minimizing sound power from vibrating shell structures. AIAA J 36:134–139

Du J, Olhoff N (2007) Minimization of sound radiation from vibrating bi-material structures using topology optimization. Struct Multidisc Optim 33:305–321

Du J, Olhoff N (2010) Topological design of vibrating structures with respect to optimum sound pressure characteristics in a surrounding acoustic medium. Struct Multidisc Optim 42:43–54

Duhring MB, Jensen JS, Sigmund O (2008) Acoustic design by topology optimization. J Sound Vib 317:557–575

Eschenauer H, Olhoff N 2001 Topology optimization of continuum structures: a review. Appl Mech Rev 54:331–389

Jog CS (2002a) Topology design of structures subjected to periodic loading. J Sound Vib 253:687–709

Jog CS (2002b) Reducing radiated sound power by minimizing the dynamic compliance. In: Proceedings of the IUTAM symposium on designing for quietness, Bangalore, India, 12–14 Dec. Kluwer, Dordrecht

Jog CS (2003) Sound reduction in external and internal domains by minimizing a single performance functional. In: Proceedings of internoise 2003. Seogwipo, South Korea

Koopman GH, Fahnline JB (1997) Designing quiet structures. Academic Press, London

Lamancusa JS (1993) Numerical optimization technique for structural-acoustic design of rectangular plates. Comput Struct 48:661–675

Ma ZD, Kikuchi N, Cheng HC (1995) Topological design for vibrating structures. Comput Methods Appl Mech Eng 121:259–280

Marburg S (2002a) A general concept for design modification of shell meshes in structural-acoustic optimization—part 1: formulation of the concept. Finite Elem Anal Des 38:725–735

Marburg S (2002b) Development in structural-acoustic optimization for passive noise control. Arch Comput Methods Eng 9(4):291–370

Marburg S (2004) A survey of applications in structural-acoustic optimization for passive noise control with a focus on optimal shell contour. Advances in dynamics and control. CRC Press, pp 205–219

Milsted MG, Zhang T, Hall RA (1993) A numerical method for noise optimization of engine structures. J Automobile Engrg 207:135–143